# The Effect of Spin-Orbit Coupling on the Polar Kerr Effect in $Sr_2RuO_4$

Joshua Robbins,[1,*] James F. Annett,[1] and Martin Gradhand[1]

[1] *H. H. Wills Physics Laboratory, University of Bristol, Tyndall Avenue, BS8 1TL, United Kingdom*

(Dated: September 15, 2017)

The polar Kerr effect arises in states with broken time-reversal symmetry and has recently been observed in a series of unconventional superconductors. In the normal state, the Kerr effect is driven by time reversal symmetry breaking of the spin system in conjunction with spin-orbit coupling. In contrast for the superconducting state the effect may arise from a chiral gap structure breaking time reversal symmetry within the orbital degree of freedom. Here, we study the interplay of both mechanisms being present simultaneously in the chiral superconducting phase of $Sr_2RuO_4$ including spin-orbit coupling. It was found that the introduction of spin-orbit coupling induces significant orbital mixing within the bandstructure. This has a profound influence on calculations of anomalous Hall transport, and thus the Kerr angle. We also compare our 3D model of $Sr_2RuO_4$ to a recent 2D model and analyse in detail which parts of the Brillouin zone predominantly contribute to the effect in both models.

## I. INTRODUCTION

The layered-perovskite compound $Sr_2RuO_4$ is considered a strong candidate for chiral $p$-wave pairing. A large amount of research has been carried out in attempts to confirm this hypothesis[? ?] , but its order parameter in the superconducting state is not yet fully understood[?] . The proposed spin triplet ($L = 1$, $S = 1$) state would be a charged analogue of the well-described superfluid A phase of $^3$He[? ?] . This chiral state breaks time-reversal symmetry (TRS), leading to a variety of anomalous phenomena such as orbital magnetism[? ?] , the quantum Hall effect[? ?] and edge currents[? ? ?] .

A further indication that TRS has been broken is the occurrence of circular dichroism[? ? ?] . The Kerr effect is a consequence of circular dichroism, it is directly measured as the difference in the reflectivity of right and left-handed, circularly polarised beams[?] . A finite Kerr signal was found experimentally in $Sr_2RuO_4$[?] , with an onset temperature equal to the superconducting critical temperature ($T_c = 1.5$ K). This provides strong evidence that TRS is broken at the superconducting transition. However, controversy remains concerning the superconducting order parameter as the edge currents predicted to accompany the chiral state have not been found[? ?] .

Many theoretical models of $Sr_2RuO_4$ were proposed following the experiment in attempts to describe an intrinsic origin of the optical effect[? ? ? ?] . These works focussed predominantly on single-band pictures and were unable to produce a quantitative prediction of the Kerr angle in the superconducting state. Subsequently, it was argued that the intrinsic effect must vanish by symmetry in a spatially homogeneous system[? ? ?] , and that the source of the Kerr rotation may be extrinsic, i.e. due to impurity scattering[? ? ? ?] .

It has since been shown, however, that the intrinsic approach to the Kerr effect can indeed produce reasonable estimates, but a multi-band model is essential to recover the effect[? ? ?] . The reason for this result is the fundamental link between the Kerr effect and the anomalous Hall transport, which in turn requires a finite Berry curvature[?] . Contributions to the Berry curvature occur at near-degeneracies and avoided crossings of different bands, meaning that the curvature is zero when only a single band is considered.

In this work, the 3D tight-binding model of $Sr_2RuO_4$ used in Ref. **?** was extended to include spin-orbit coupling (SOC). We will discuss its implications in detail, benchmark its influence with respect to experimental results, and compare our results qualitatively as well as quantitatively to other model approaches. The findings will be compared with a recent 2D model proposed by Scaffidi and Simon[?] , which attempts to reconcile TRS-breaking with the absence of edge currents as observed in experiments. The numerical method will be briefly reviewed in section II. In section III, the different models are compared with respect to their quantitative description of the experimentally found Kerr effect as well as the heat capacity in the superconducting state.

## II. METHODS

### A. Model of the Normal State and Spin-Orbit Coupling

The normal state tight-binding Hamiltonian

$$H^{tb}(\mathbf{k}) = \begin{pmatrix} H_{aa}(\mathbf{k}) & H_{ab}(\mathbf{k}) & H_{ac}(\mathbf{k}) \\ H_{ab}(\mathbf{k}) & H_{bb}(\mathbf{k}) & H_{bc}(\mathbf{k}) \\ H_{ac}(\mathbf{k}) & H_{bc}(\mathbf{k}) & H_{cc}(\mathbf{k}) \end{pmatrix}$$

is constructed from the Ru 4$d$ $d_{xy}$, $d_{xz}$ and $d_{yz}$ orbitals, denoted $a$, $b$ and $c$ respectively[?] . The matrix elements

are defined as the following:

$$\begin{aligned}
H_{aa} &= \epsilon_a + 2t(\cos(k_x) + \cos(k_y)) \\
&\quad + 4t'(\cos(k_x)\cos(k_y)) \\
H_{bb} &= \epsilon_b + 2(t_b^x\cos(k_x) + t_c^x\cos(k_y)) \\
&\quad + 8t_b^\perp\,(\cos(k_x/2)\cos(k_y/2)\cos(ck_z/2)) \\
H_{cc} &= \epsilon_b + 2(t_c^x\cos(k_x) + t_b^x\cos(k_y)) \\
&\quad + 8t_b^\perp\,(\cos(k_x/2)\cos(k_y/2)\cos(ck_z/2)) \\
H_{ab} &= 8t_{ab}^\perp\,(\cos(k_x/2)\sin(k_y/2)\sin(ck_z/2)) \\
H_{ac} &= 8t_{ab}^\perp\,(\sin(k_x/2)\cos(k_y/2)\sin(ck_z/2)) \\
H_{bc} &= 4t_{bc}\sin(k_x)\sin(k_y) \\
&\quad + 8t_{bc}^\perp\,(\sin(k_x/2)\sin(k_y/2)\cos(ck_z/2))
\end{aligned}$$

where $\epsilon_a$ is the on-site energy and $t$ and $t'$ are hopping parameters corresponding to nearest and next-nearest neighbours respectively for the $d_{xy}$ orbital. Similar terms are defined for the $d_{xz}$ and $d_{yz}$ orbitals, in addition to inter-orbital hoppings $t_{ab}^\perp$, $t_{bc}^\perp$, and $t_{bc}$. The on-site and hopping parameters were fine-tuned so as to reproduce the experimentally found Fermi surface areas[?], bandwidth[?] and cyclotron masses[?] (the tight-binding parameters used are listed in Table 1). The only point we would like to note here, is that the tight-binding model presented in Ref. [?] produces a bandwidth of roughly 0.7 eV (see Figure 1 a). This is in agreement with the Fermi surface measured in de Haas-van Alphen experiments[?] as well as direct ARPES results giving a bandwidth of $\sim$1 eV[?]. Furthermore, it agrees with other tight-binding fits. This is in stark contrast to ab initio results[? ?] where the bandwidth is significantly larger than in experiments[?]. This comparison leads to a band renormalization by a factor of about 1/4 which will be highly relevant for the discussion to follow.

This model has been used previously to account for the Kerr effect and various other aspects such has the heat capacity. However, in the past the SOC has been ignored. Given that it is the SOC which is, in combination with time-reversal symmetry breaking, responsible for the Kerr effect in the normal state, this seems like a problematic approximation. Furthermore, for the quantitative consideration of edge currents and the orbital moment the incorporation of SOC appears to be vital. Here, we introduce Pauli spin-orbit coupling by taking an on-site approximation. The spin-orbit Hamiltonian is given in orbital representation as[?]:

$$H^{so} = \lambda\sum_i \mathbf{l_i}\cdot\mathbf{s_i} = \lambda\begin{pmatrix} 0 & 0 & 0 & 0 & -i & 1 \\ 0 & 0 & -i & i & 0 & 0 \\ 0 & i & 0 & -1 & 0 & 0 \\ 0 & -i & -1 & 0 & 0 & 0 \\ i & 0 & 0 & 0 & 0 & i \\ 1 & 0 & 0 & 0 & -i & 0 \end{pmatrix} \qquad (1)$$

where the 6 matrix indices account for the 3 orbitals plus spin.

In the literature, there is an extended controversy concerning the magnitude of the spin-orbit coupling parameter $\lambda$. Some authors have suggested that $\lambda \lesssim 50$ meV[? ?], while orbital excitation spectra suggest a value as high as 200 meV[?].

From ab initio calculations, the SOC parameter within our notation can be inferred to be $\lambda \sim 50$ meV. This leads to an effective splitting of 100 meV at the $\Gamma$ point[?]. Considering the ab initio band width, our tight-binding model including SOC $\lambda \sim 50$ meV recovers that splitting as can be seen in Fig. 1 b. However, in the case of the experimentally found bandwidth, spin-orbit coupling of that size leads to a complete rearrangement of the Fermi surface. It is impossible to reconcile such large SOC parameter with the experimentally found Fermi surface. This is due to the significant band renormalization increasing the effective SOC on the energy scale set by the hopping parameter $t$. In light of this, it appears natural to apply the same renormalization to the SOC constant $\lambda$ as for the hopping parameters $t$. Scaling it by 1/4 leads to $\lambda = 12.5$ meV which provides a Fermi surface and effective masses in reasonable agreement to experiment. The resulting bandstructure is shown in Fig. 4 c.

### A. Superconducting State

In order to describe the superconducting state, we solve the Bogoliubov-de Gennes (BdG) equation self-consistently in the tight-binding representation[?]:

$$\begin{pmatrix} H(\mathbf{k}) & \hat{\Delta}(\mathbf{k}) \\ \hat{\Delta}^\dagger(\mathbf{k}) & -H^*(-\mathbf{k}) \end{pmatrix}\begin{pmatrix} u(\mathbf{k}) \\ v(\mathbf{k}) \end{pmatrix} = E\begin{pmatrix} u(\mathbf{k}) \\ v(\mathbf{k}) \end{pmatrix} \qquad (2)$$

where $H(\mathbf{k}) = H^{tb}(\mathbf{k}) + H^{so}$ and the gap function ($\Delta$) has the chiral structure $\mathbf{d}\sim(k_x \pm ik_y)\hat{\mathbf{z}}$[?].

We consider the superconducting state in a fully three-dimensional fashion and enforce superconducting gaps on all three bands at the Fermi surface. The superconductivity in the $d_{xz}$ and $d_{yz}$ orbitals, mainly contributing to the $\alpha$ and $\beta$ bands, is induced by nearest-neighbour pairing terms mediated via an out-of-plane interaction. This is indeed of the same p-wave symmetry, corresponding to the group representation $E_u$, as the chiral pairing in the $d_{xy}$ orbital. In our phenomenological approach, the interlayer pairing interaction for the $d_{xz}$ and $d_{yz}$ orbitals is tuned in conjunction with the in-plane pairing for the $d_{xy}$ orbital, such that the superconducting transition occurs simultaneously for all three bands at the correct temperature of 1.5 K. The microscopic origin of such an interlayer coupling is currently unknown, but interlayer exchange of magnetic fluctuations is a possible origin[? ?]. In addition, the existence of the chiral p-wave pairing in the $d_{xz}$ and $d_{yz}$ channel subtly depends on this orbital dependent pairing. If we reduce this coupling by only 30%, the self-consistent solution obtained displays superconductivity driven almost entirely by the $d_{xy}$ orbital. This approach leads naturally to the occurrence

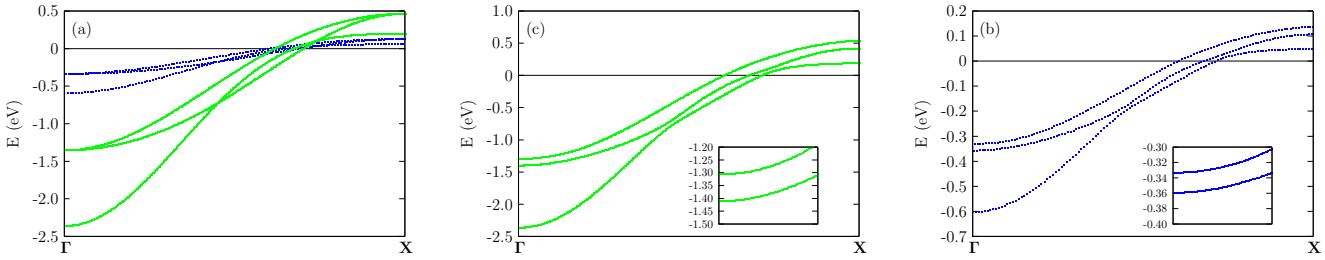


FIG. 1. Tight binding bandstructure along the [110] direction for a) without SOC comparing the large band width (first principles) to the renormalized band width (experimental), b) including SOC for the large bandwidth and c) including SOC for the renormalized bandstructure.

of horizontal line nodes at $\pm\pi/c$ along the $z$-axis.[?] This nodal structure accurately accounts for the specific heat observed experimentally in $Sr_2RuO_4$ (see Section III).

The resulting gap is of similar order on all three bands, being slightly larger on the $\gamma$ band which is derived predominantly from the $a$ orbital. The gap function for this orbital is given by:

$$\Delta_{aa}^{\uparrow\downarrow}(\mathbf{k}) = \eta_{aa}^{U}\left(\sin(k_x) + i\sin(k_y)\right) \tag{3}$$

where the parameter $U$ determines the strength of the pairing interaction.

For the $b$ and $c$ orbitals, the gap function takes the following form:

$$\Delta_{bb}^{\uparrow\downarrow}(\mathbf{k}) = \eta_{bb}^{U'}(\sin(k_x/2)\cos(k_y/2)\cos(ck_z/2) + i\,\eta_{cc}^{U'}\cos(k_x/2)\sin(k_y/2)\cos(ck_z/2)) \tag{4}$$

with a similar term for $\Delta_{cc}$. These two terms (as well as the inter-orbital term $\Delta_{bc}$) are dependent on a different interaction parameter $U'$, mediated via out-of-plane hopping. For a thorough discussion of the pairing terms and the appropriate symmetry considerations, we refer the reader to the papers[? ? ?]. It is important to note that we solve the above equations fully self-consistently, iteratively calculating $\eta_{aa}^{U}$, $\eta_{bb}^{U'}$, and $\eta_{cc}^{U'}$ from the solution of Eq. 2 until self-consistency is reached[?].

In order to account for the inclusion of SOC, the previously used pairing interaction parameters $U$ and $U'$[?] had to be adjusted to derive the correct critical temperature $T_c = 1.5$ K (see Table I).

### B. Transport Calculations

In order to study the Kerr effect, we must consider the conductivity of the state due to interaction with an incident photon. If the state breaks TRS (and is thus dichroic) there is an off-diagonal response, i.e. a non-zero optical Hall conductivity ($\sigma_{xy}$). An expression for $\sigma_{xy}$ was derived following a linear-response approach[? ?], giving its real and imaginary components as:

$$\mathrm{Im}[\sigma_{xy}(\omega)] = \frac{\pi^2 e^2}{2\omega V m^2}\sum_{n,n',\mathbf{k}} f(E_n(\mathbf{k}))\left[1 - f(E_{n'}(\mathbf{k})\right] \times \left(\left|\langle\psi_{n'\mathbf{k}}\left|H_I(\boldsymbol{\epsilon_L})\right|\psi_{n\mathbf{k}}\rangle\right|^2 - \left|\langle\psi_{n'\mathbf{k}}\left|H_I(\boldsymbol{\epsilon_R})\right|\psi_{n\mathbf{k}}\rangle\right|^2\right) \times \delta(E_n(\mathbf{k}) - E_{n'}(\mathbf{k}) - \hbar\omega) \tag{5}$$

$$\mathrm{Re}[\sigma_{xy}(\omega)] = \frac{e^2\hbar}{Vm^2}\sum_{n,n',\mathbf{k}} f(E_n(\mathbf{k}))\left[1 - f(E_{n'}(\mathbf{k})\right] \times \frac{\left(\left|\langle\psi_{n'\mathbf{k}}\left|H_I(\boldsymbol{\epsilon_L})\right|\psi_{n\mathbf{k}}\rangle\right|^2 - \left|\langle\psi_{n'\mathbf{k}}\left|H_I(\boldsymbol{\epsilon_R})\right|\psi_{n\mathbf{k}}\rangle\right|^2\right)}{\left(E_n(\mathbf{k}) - E_{n'}(\mathbf{k})\right)^2 - (\hbar\omega)^2} \tag{6}$$

where $\psi_{n\mathbf{k}}$ are Bloch wavefunctions and $H_I(\boldsymbol{\epsilon_{L/R}})$ is the Hamiltonian describing the interaction with a left/right-handed photon.[? ? ?]

Converting to the tight-binding basis, the matrix elements of $H_I$ are given by:

$$\langle n'\mathbf{k}\left|H_I(\boldsymbol{\epsilon_L})\right|n\mathbf{k}\rangle = \frac{m\boldsymbol{\epsilon}^*_{\boldsymbol{L/R}}}{i\hbar}\begin{pmatrix}u_{n'}(\mathbf{k})\\ v_{n'}(\mathbf{k})\end{pmatrix}^{\dagger} \times \begin{pmatrix}\nabla_{\mathbf{k}}H(\mathbf{k}) & 0\\ 0 & \nabla_{\mathbf{k}}H(\mathbf{k})\end{pmatrix}\begin{pmatrix}u_n(\mathbf{k})\\ v_n(\mathbf{k})\end{pmatrix} \tag{7}$$

The Kerr angle is then directly related to the Hall conductivity by[?]:

$$\theta_K(\omega) = \frac{1}{\epsilon_0\omega}\mathrm{Im}\left[\frac{\sigma_{xy}(\omega)}{n(\omega)[n^2(\omega) - 1]}\right] \tag{8}$$

where $n(\omega)$ is the complex refractive index.

Following this approach, it has been previously demonstrated that a finite Kerr effect can be found intrinsically in the superconducting state[? ?]. The influence of spin-orbit coupling on these results will be presented in section III.

### C. Two-Dimensional Model

To compare our results using the above model to other theoretical approaches, we briefly introduce a 2D model put forward by Scaffidi and Simon[?] . The main aim of their model was to accommodate theoretical predictions[? ? ?] with the absence of edge currents in experimental investigations[? ?] . In order to achieve this, they performed functional renormalization group calculations on the Fermi surface. The results of this, transformed to real space, leads to effective longer-ranged pairing terms going beyond the nearest neighbour pairing that we have considered so far. The derived gap has the following form:

$$\Delta^{\mathrm{2D}}_{aa}(\mathbf{k}) = \eta'_{aa}\left(\sin(k_x) + i\sin(k_y)\right) + \eta''_{aa}\left(\sin(k_x)\cos(k_y) + i\sin(k_y)\cos(k_x)\right) + \eta'''_{aa}\left(\sin(3k_x) + i\sin(3k_y)\right) \quad (9)$$

$$\Delta^{\mathrm{2D}}_{bb}(\mathbf{k}) = \eta'_{bb}\left(\sin(k_x)\cos(k_y)\right) + \eta''_{bb}\left(\sin(3k_x)\right) \quad (10)$$

$$\Delta^{\mathrm{2D}}_{cc}(\mathbf{k}) = \eta'_{bb}\left(i\sin(k_x)\cos(k_y)\right) + \eta''_{bb}\left(i\sin(3k_x)\right) \quad (11)$$

It was demonstrated that including these terms results in a different Chern number, which is shown to suppress edge currents.

Although it was shown that this model can produce a reasonable estimate of the heat capacity jump at $T_c$[?] , the effects of the new order parameter on transport properties and the power law behaviour of the specific heat were not discussed by Scaffidi and Simon. Here, we aim to assess the viability of such a model to produce the experimentally found electronic properties of $Sr_2RuO_4$. The results of the two models in relation to experiment will be discussed in section III. In contrast to the approach taken here, in Ref.[?] the BdG equation was not solved as a function of temperature and all results were obtained for T = 0. Therefore, we model the temperature dependence for the 2D case by $\Delta(T) = \Delta(0)\sqrt{1-(T/T_c)}$ in our calculations presented below.

## III. RESULTS

Before we start to analyse the specific heat and transport properties of the superconducting state, we would like to briefly highlight the dominant implications of SOC on the electronic structure of the normal state of $Sr_2RuO_4$. The three Fermi surface sheets can be seen in Fig. 2, which displays a series of orbitally-resolved Bloch spectra. The addition of spin-orbit coupling does not significantly alter the areas enclosed by these sheets. However, the individual contributions of each orbital to the electronic states are strongly affected by SOC, leading to a significant mixing of the orbital character within the different bands. This effect is most prominent at the near degeneracies along the 110 direction, where all orbitals contribute similarly to the three bands.

When SOC is included the $d_{xy}$ orbital is no longer con-

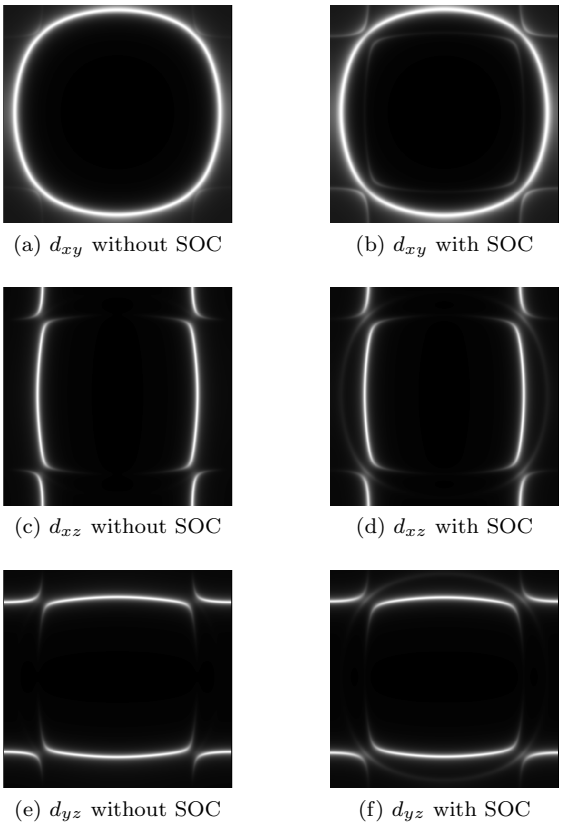

(a) $d_{xy}$ without SOC (b) $d_{xy}$ with SOC

(c) $d_{xz}$ without SOC (d) $d_{xz}$ with SOC

(e) $d_{yz}$ without SOC (f) $d_{yz}$ with SOC

FIG. 2. a)-f) show the individual contributions of the $d_{xy}$, $d_{xz}$ and $d_{yz}$ orbitals respectively, with (right) and without (left) the inclusion of SOC.

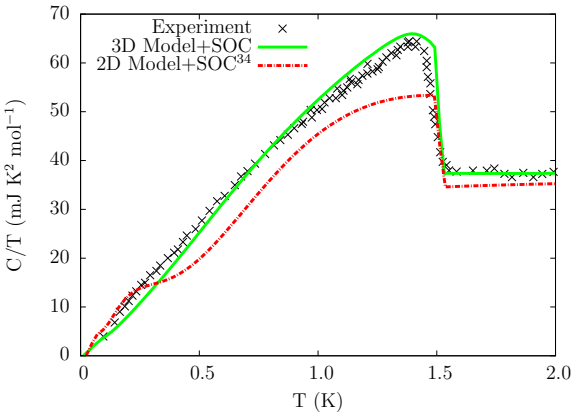


FIG. 3. Heat capacity calculation alongside experimental data[?] .

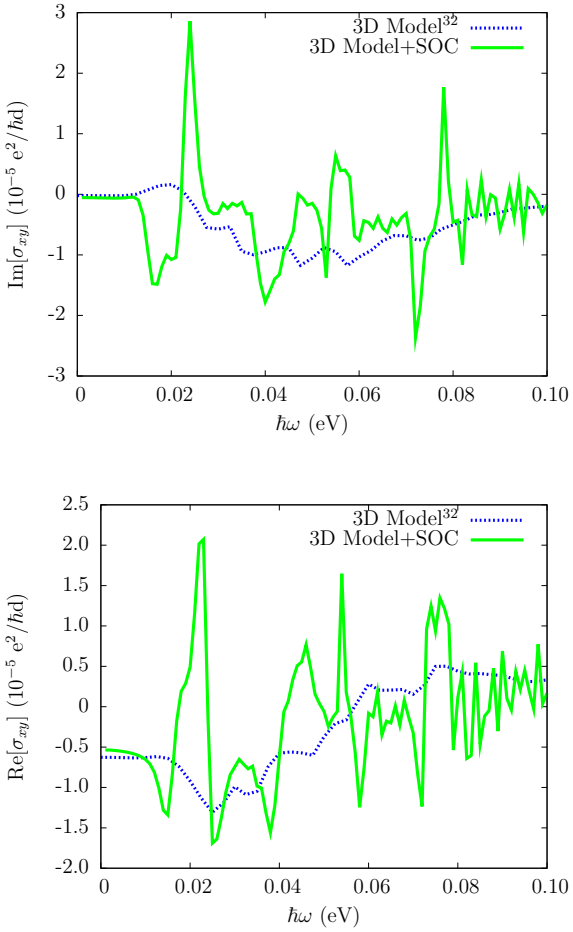


FIG. 4. The imaginary (upper panel) and real (lower panel) component of the optical Hall conductivity in the low-frequency regime, for the 3D model with and without SOC.

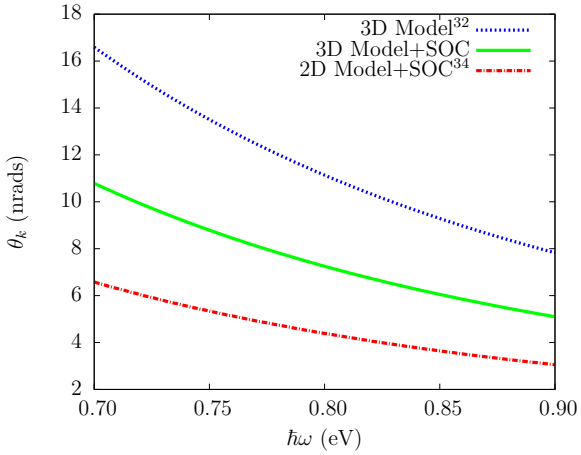


FIG. 5. Estimated Kerr angle in the high-frequency regime with and without SOC.

fined to only the circular $\gamma$ band, but also contributes to the $\alpha$ pockets and central $\beta$ band. Similar mixing occurs for the $d_{xz}$ and $d_{yz}$ bands and has been reported previously[?] . In agreement with our results, the addition of SOC and the subsequent orbital mixing were reported to have a negligible influence on Fermi surface areas. However, given the fact that the Berry curvature[?] driving the intrinsic Kerr effect is mitigated via the hybridization of bands, this mixing is expected to have profound effects on the Kerr effect in $Sr_2RuO_4$.

Having solved the BdG equation for the 3D model self-consistently, the heat capacity, using standard expressions[?] , was calculated (see Fig. 3). A remarkably good fit with experimental data is observed, in both the normal and superconducting phases, with the transition marked by the characteristic jump at $T_c$. This is in agreement with previous findings neglecting spin-orbit coupling[?] .

In both cases, the 3D as well as the 2D model, the slope at low temperatures is in very good agreement to the experiment. However, for higher temperatures the 2D model deviates from the experimental curve which might be induced by the lack of self-consistency in this case.

Finally, following the approach outlined in II.B, the optical Hall conductivity was computed. In Fig. 4, this is compared with calculations ignoring SOC. In the low-frequency regime ($0-0.1$ eV), SOC clearly has a severe impact on the behaviour of $\sigma_{xy}$, showing rich structure below 0.1 eV.

In the high-frequency regime ($0.7-0.9$ eV), the imaginary component of $\sigma_{xy}$ vanishes and the addition of SOC simply results in a shift in the real part. This leads to an estimated Kerr angle of 6.3 nrads at 0.8 eV, the frequency used experimentally, compared to the 12 nrads obtained in the previous model. Qualitatively, the reduction induced by SOC can be understood by the fact that it transfers orbital magnetic order, which is driving the Kerr effect, to the spin degree of freedom. This is in contrast to the normal ferromagnetic state where it is the SOC which transfers spin magnetic order to the orbital degrees of freedom to induce the Kerr effect. Similar results are obtained for the 2D model showing a slight reduction but overall the same order of magnitude. The theoretical values compare to experimentally-obtained results, which are in the region 60-90 nrads. While there is a notable discrepancy between computed and experimental values, this estimation is orders of magnitude closer than previous findings[? ? ? ?] . It should also be stressed that these values are calculated by taking a rough estimation of the complex refractive index $n(\omega)$. The methods taken to estimate $n(\omega)$ and the impact of this approximation on the results are discussed in more detail in Ref.[?] .

## IV. DISCUSSION

The occurrence of intrinsic anomalous Hall transport in any electron system including in the superconducting state requires the bands to display a finite Berry curvature.[?] Such a curvature is induced and enhanced by near-degeneracies in the quasi-particle bandstructure, but will be divergent at actual degeneracies. The various avoided crossings induced by SOC are therefore significant in our calculations of $\sigma_{xy}$.

The orbital mixing displayed in Fig. 2 strongly influences the photon frequencies for which inter-orbital transitions can occur. These transitions are the key source of Berry curvature and thus the Kerr effect. The huge amount of structure in the low-frequency regime, induced by SOC with a relatively small coupling parameter, demonstrate that the spin-orbit interaction can not be ignored when studying the frequency dependence of the Kerr effect.

Over all, the two-dimensional model by Scaffidi and Simon[?] describes the physical observables such as the specific heat and Kerr angle with results similar to our full 3D model. In the 2D case, the longer-range pairing terms included induce the required nodal structure, in contrast to the out of plane interaction in our full 3D model. The power law for $T << T_c$ correctly reproduces the experimental findings and any deviations for higher temperatures have to be considered with caution since we are not enforcing self-consistency for this model. Ultimately, it would be interesting to incorporate these higher order pairing terms into our self-consistent 3D model in order to more accurately quantify the effects of the additional terms.

Finally, in Fig. 6 we present heat maps of the $k_x - k_y$ resolved optical conductivity as well as specific heat for the full 3D-model in order to highlight the driving mechanisms behind the different physical observables. For this figure we choose $k_z = 0$. Evidently, the contributions to the Hall conductivity and the specific heat stem from rather distinct regions in the Brillouin zone. Whereas the contributions to the Hall conductivity peak around the near degeneracies along the 110 directions this is different for the specific heat. In the latter case the contributions are almost uniformly distributed on the Fermi surface of the $d_{xz}$ and $d_{yz}$ orbitals of $Sr_2RuO_4$ with the SOC having virtually no effect. In contrast the SOC changes the picture for the Hall conductivity by inducing a stronger band mixing as well as further avoided crossings. This leads to much more fine structure in the otherwise very localised contributions. Even more importantly we now see contributions from the predominantly $d_{xy}$ band due to the additional orbital character mixing as shown in Fig. 2. However, this band contributes with the opposite sign which creates much more fine structure over all. In contrast, the low temperature specific heat is determined by the line nodes in the quasi-particle bandstructure on the predominantly $d_{xz}$ and $d_{yz}$ band which is clearly visible comparing the heat maps to the Bloch spectral function in Fig. 2.

In summary, we have presented a detailed analysis of the effect of spin-orbit coupling on the superconducting state of $Sr_2RuO_4$ and its implication on observables such as the specific heat and the Kerr effect. Despite the fact that SOC fundamentally changes the orbital contributions to each band, which ultimately is one of the crucial ingredients to the Kerr effect, the quantitative implications at the experimentally used frequency is rather limited. The main argument for this is that the rather high frequency considered in the experiment is significantly higher than the natural frequencies of the system for which the effect is dominant. These frequencies are between $0.01 - 0.1$ eV and are determined by the inter-orbital hybridization gaps induced in the normal state. Nevertheless, the importance of the consideration of the SOC comes from the understanding that it is SOC which is responsible for the Kerr effect in the normal state in conjunction with the time reversal symmetry breaking induced by ordinary spin-induced ferromagnetism. However, in this study of the chiral pairing in superconducting $Sr_2RuO_4$ the chiral gap structure takes both roles breaking the time reversal symmetry via orbital ordering as well as breaking the crucial mirror symmetries to allow for a finite Hall conductivity. It implies that the complex gap function takes the role of time reversal symmetry breaking as well as the "spin-orbit coupling" at the same time which leads to only minor quantitative effects considering the normal state SOC as well. Nevertheless, were we able to probe lower frequencies $0.01 - 0.1$ eV we showed that the effect of spin-orbit coupling changes the Hall conductivity dramatically leading to a significant effect on the Kerr angle.

Finally, we compare the calculations to a distinct 2D order parameter put forward to account for the particular findings in $Sr_2RuO_4$ such as the vanishing of any edge currents in the superconducting state. Our quantitative analysis suggests that, on the level of the currently available data, we cannot fundamentally decide between the two order parameters and further experiments are needed to make a distinction. Clearly, it would be important to extend the 2D model to a full self-consistent calculation possibly combining both order parameters.

Extending this work we would like to point to two additional aspects. The first was highlighted before and refers to the complex refractive index required to quantitatively gauge the magnitude of the Kerr angle. This is not well accounted for within our model and has to be approximated from experimental results. This induces a large scale of uncertainty in our quantitative predictions. Further work is required to quantify its frequency dependence more accurately before detailed quantitative comparisons to the experiments are possible. Secondly, naturally our work lends itself to the quantitative analysis of the orbital magnetic moment in the superconducting states for which only rough estimates exist so far. All experimental efforts in this direction relied on crude approximations varying by order of magnitudes. The same

is true for the estimates of edge currents which are simply a reincarnation of the orbital magnetic moment in finite size samples. However, our extension and thorough analysis of the effect of spin-orbit coupling prepares the ground for a quantitative analysis of this long standing problem.

## ACKNOWLEDGMENTS

This work was carried out using the computational facilities of the Advanced Computing Research Centre, University of Bristol - http://www.bris.ac.uk/acrc/. J.R. acknowledges support via the CMP-CDT funded by EPSRC and J.F.A. via EPSRC grant EP/P007392/1. M.G. acknowledges financial support from the Leverhulme Trust via an Early Career Research Fellowship (ECF-2013-538).

* jr9334@bristol.ac.uk

A. P. Mackenzie and Y. Maeno, Rev. Mod. Phys. **75**, 657 (2003).
Y. Maeno, T. M. Rice, and M. Sigrist, Physics Today **54**, 42 (2001).
J. F. Annett, G. Litak, B. L. Györffy, and K. I. Wysokiǹski, Phys. Rev. B **73**, 134501 (2006).
A. J. Leggett, Rev. Mod. Phys. **47**, 331 (1975).
A. J. Leggett, Phys. Rev. Lett. **29**, 1227 (1972).
T. Thonhauser, D. Ceresoli, D. Vanderbilt, and R. Resta, Phys. Rev. Lett. **95**, 137205 (2005).
J. F. Annett, B. L. Györffy, and K. I. Wysokiǹski, New Journal of Physics **11**, 055063 (2009).
A. Furusaki, M. Matsumoto, and M. Sigrist, Phys. Rev. B **64**, 054514 (2001).
N. Read and D. Green, Phys. Rev. B. **61**, 10267 (2000).
M. Matsumoto and M. Sigrist, J. Phys. Soc. Jpn. **68**, 994 (1999).
M. Stone and R. Roy, Phys. Rev. B **69**, 184511 (2004).
W. Huang, S. Lederer, E. Taylor, and C. Kallin, Phys. Rev. B **91**, 094507 (2015).
S. K. Yip and J. A. Sauls, J. Low Temp. Phys. **86**, 257 (1992).
K. Capelle, E. K. U. Gross, and B. L. Györffy, Phys. Rev. Lett. **78**, 3753 (1997).
K. Capelle, E. K. U. Gross, and B. L. Györffy, Phys. Rev. B. **58**, 473 (1998).
A. Kapitulnik, J. Xia, E. Schemm, and A. Palevski, New Journal of Physics **11**, 055060 (2009).
J. Xia, Y. Maeno, P. T. Beyersdorf, M. M. Fejer, and A. Kapitulnik, Phys. Rev. Lett. **97**, 167002 (2006).
J. R. Kirtley, C. Kallin, C. W. Hicks, E.-A. Kim, Y. Liu, K. A. Moler, Y. Maeno, and K. D. Nelson, Phys. Rev. B **76**, 014526 (2007).
C. W. Hicks, J. R. Kirtley, T. M. Lippman, N. C. Koshnick, M. E. Huber, Y. Maeno, W. M. Yuhasz, M. B. Maple, and K. A. Moler, Phys. Rev. B **81**, 214501 (2010).
V. M. Yakovenko, Phys. Rev. Lett. **98**, 087003 (2007).
V. P. Mineev, Phys. Rev. B. **76**, 212501 (2007).
R. Roy and C. Kallin, Phys. Rev. B. **77**, 174513 (2008).
"References 20 and 21 produced reasonable estimates of the Kerr angle. However, the equations used by these authors were later shown in Ref. 22 to be inaccurate in the superconducting state,".
R. M. Lutchyn, P. Nagornykh, and V. M. Yakovenko, Phys. Rev. B. **77**, 144516 (2008).
V. P. Mineev, J. Phys. Soc. Jpn. **81**, 093703 (2012).
W. Kim, F. Marsiglio, and C. S. Ting, Phys. Rev. Lett. **100**, 227003 (2008).
J. Goryo, Phys. Rev. B. **78**, 060501(R) (2008).
R. M. Lutchyn, P. Nagornykh, and V. M. Yakovenko, Phys. Rev. B. **80**, 104508 (2009).
J. Goryo, Mod. Phys. Lett. B **24**, 2831 (2010).
E. Taylor and C. Kallin, Phys. Rev. Lett. **108**, 157001 (2012).
K. I. Wysokiǹski, J. F. Annett, and B. L. Györffy, Phys. Rev. Lett. **108**, 077004 (2012).
M. Gradhand, K. I. Wysokiǹski, J. F. Annett, and B. L. Györffy, Phys. Rev. B. **88**, 094504 (2013).
M. Gradhand and J. F. Annett, J. Phys.: Condens. Matter **26**, 274205 (2014).
T. Scaffidi and S. H. Simon, Phys. Rev. Lett. **115**, 087003 (2015).
A. P. Mackenzie, S.-I. Ikeda, Y. Maeno, T. Fujita, S. R. Julian, and G. G. Lonzarich, J. Phys. Soc. Jpn. **67**, 385 (1998).
T. Yokoya, A. Chainani, T. Takahashi, H. Ding, J. C. Campuzano, H. Katayama-Yoshida, M. Kasai, and Y. Tokura, Phys. Rev. B **54**, 13311 (1996).
A. P. Mackenzie, S. R. Julian, A. J. Diver, G. J. McMullan, M. P. Ray, G. G. Lonzarich, Y. Maeno, S. Nishizaki, and T. Fujita, Phys. Rev. Lett. **76**, 3786 (1996).
V. B. Zabolotnyy, D. V. Evtushinsky, A. A. Kordyuk, T. K. Kim, E. Carleschi, B. P. Doyle, R. Fittipaldi, M. Cuoco, A. Vecchione, and S. V. Borisenko, J. Electron Spectrosc. Relat. Phenom. **191**, 48 (2013).
P. K. de Boer and R. A. de Groot, Phys. Rev. B **59**, 9894 (1999).
M. W. Haverkort, I. S. Elfimov, L. H. Tjeng, G. A. Sawatzky, and A. Damascelli, Phys. Rev. Lett. **101**, 026406 (2008).
T. Tanaka, H. Kontani, M. Naito, D. S. Hirashima, K. Yamada, and J. Inoue, J. Phys. Chem. Solids **69**, 3250 (2008).
Y. Yanase, S. Takamatsu, and M. Udagawa, J. Phys. Soc. Jpn. **83**, 061019 (2014).
Y. Yanase and M. Ogata, J. Phys. Soc. Jpn. **72**, 673 (2003).
C. G. Fatuzzo, M. Dantz, S. Fatale, P. Olalde-Velasco, N. E. Shaik, B. Dalla Piazza, S. Toth, J. Pelliciari, R. Fittipaldi, A. Vecchione, N. Kikugawa, J. S. Brooks, H. M. Rønnow, M. Grioni, C. Rüegg, T. Schmitt, and J. Chang, Phys. Rev. B **91**, 155104 (2015).
J. B. Ketterson and S. N. Song, *Superconductivity* (Cambridge University Press, 1999).
I. Eremin, D. Manske, J. R. Tarento, and K. H. Bennemann, Journal of Superconductivity: Incorporating Novel Magnetism **15**, 447 (2002).

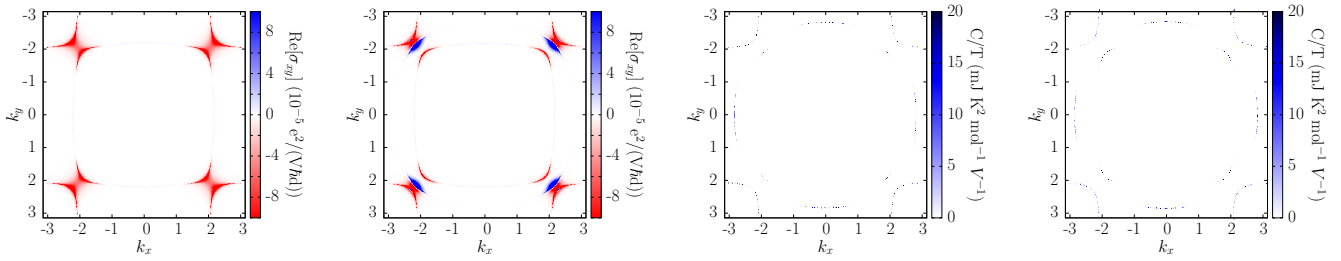


FIG. 6. The $k_x - k_y$ resolved optical conductivity (the left two heat maps) and the $k_x - k_y$ resolved specific heat (the right two heat maps) for $k_z = 0$ dependence. In each case we first show the case without and than with SOC. The temperature for the specific heat is effectively zero (T=0.16K), where only the quasiparticle bands dominate the effect. Whereas for the conductivity the contributions come predominantly from a small area along the 110 direction where the band mixing is large, for the specific heat these contributions are arising from the line nodes on the $d_xz$ and $d_{yz}$ almost uniformly.


I. Eremin, D. Manske, S. G. Ovchinnikov, and J. F. Annett, Ann. Phys. (Leipzig) **13**, 149 (2004).

J. F. Annett, G. Litak, B. L. Györffy, and K. I. Wysokiǹski, Phys. Rev. B **66**, 134514 (2002).

Y. Hasegawa, K. Machida, and M. Ozaki, J. Phys. Soc. Jpn. **69**, 336 (2000).

R. M. White and T. Geballe, *Long Range Order in Solids* (Academic Press, New York, 1979).

T. Scaffidi, J. C. Romers, and S. H. Simon, Phys. Rev. B **89**, 220510(R) (2014).

S. Nishizaki, Y. Maeno, and Z. Mao, J. Phys. Soc. Jpn. **69**, 572 (2000).

T. Oguchi, J. Phys. Soc. Jpn. **78**, 044702 (2009).

| $\epsilon_a$ | $\epsilon_b$ | $t$ | $t'$ | $t_b^x$ | $t_c^x$ | $t_b^\perp$ | $t_{ab}^\perp$ | $t_{bc}$ | $t_{bc}^\perp$ | $U$ | $U'$ |
|---|---|---|---|---|---|---|---|---|---|---|---|
| -131.82 | -116.15 | -81.62 | -36.73 | -109.37 | -6.56 | 0.26 | -1.05 | -8.75 | -1.05 | 41.99 | 52.69 |

TABLE I. The numerical parameters for the tight-binding model of $Sr_2RuO_4$ and the interaction parameters describing the superconducting phase in units of meV.